Solar RRL
www.solar-rrl.com

Enhancing Photovoltaic Performance of Aromatic Ammonium-based Two-Dimensional Organic-Inorganic Hybrid Perovskites via Tuning CH···π Interaction

*Liang Yan, Jun Hu, Ninghao Zhou, Andrew M. Moran, and Wei You**

Phenethylammonium (PEA)-based 2D perovskite is an interesting example of 2D perovskites, serving as the gateway for further introduction of functional conjugated organic cations into 2D perovskites for a variety of applications, for example, photovoltaics. However, the efficiency of photovoltaic devices based on PEA 2D perovskites only achieved ≈7% for $<n>=3$, which was significantly lower than that achieved for other cation-based 2D perovskites. Here, by introducing propyl ammonium (C3A) into the PEA-based 2D perovskites, the device efficiency is improved to ≈10% for 1:1 C3A:PEA-based 2D perovskites ($<n>=3$). Further investigation reveals that tuning the CH···π interaction (between C3A and PEA or between two PEA molecules) can have multiple beneficial impacts on such modified 2D perovskites, including a) removal of undesirable $n=1$ phase, b) lowering the density of trap states, and c) achieving larger crystalline grains. Additionally, after substitution with 50% C3A, other aromatic ammonium cation-based 2D perovskites ($<n>=3$) also show similar efficiency enhancement in their photovoltaic devices, thus exhibiting the general applicability of this method. The results of this study highlight that the strategic tuning of non-covalent interactions (such as CH···π interaction) is a viable and important method to further develop 2D perovskites for photovoltaics.

1. Introduction

Though structurally closely related to three-dimensional (3D) perovskites (e.g., $CH_3NH_3PbI_3$, $MAPbI_3$), two-dimensional (2D) Ruddlesden-Popper type perovskites – with a formula of $A_2B_{n-1}Pb_nI_{3n+1}$ – have their own unique properties,[1–3] due to the incorporation of large organic cations that separate the metal halide octahedra layers (e.g., PbI_6^{4-}). Generally, A stands for the large spacer cation; B is usually a small cation such as methylammonium (MA), formamidinium (FA), or Cs^+; and n is the number of metal halide octahedra layers between the organic cation spacer layers. Though in principle, n could be any integer, here we limit n to small values ($n \leqslant 5$) for 2D perovskites because for $n > 5$, the "2D" perovskites are much more similar to 3D structures.[1]

The rising interest for 2D perovskites perhaps comes from their inherently better stability than that of 3D perovskites, mainly due to the large formation energy of the former.[4] Thus, many research groups have attempted to apply 2D perovskites to passivate either the surface or grain boundaries of 3D perovskites,[5,6] aiming to achieve better stability while maintaining desirable properties of the original 3D perovskites, e.g., high photovoltaic (PV) efficiency. In addition, the unique quantum well structure of 2D perovskites and chemical adjustability of organic cations offer prospects for other applications such as light-emitting diode (LED),[7,8] field-effect transistor (FET),[9–12] among others.[1,13]

Directly applying 2D perovskites for solar cells has met a serious challenge however, because their layer structures tend to adopt a parallel orientation to the substrate, and these insulating organic spacer cations (A in $A_2B_{n-1}Pb_nI_{3n+1}$) would prevent charge transport perpendicular to the substrate.[14] A breakthrough emerged in 2016, when Tsai et al. introduced a hot casting method,[15] which appears to realign the metal halide octahedra layer to be perpendicular to the substrate, thereby leading to an observed efficiency of as high at 12.5% and much improved stability. Since then, much more progress has been made in the development of 2D perovskites ($n \leqslant 5$) for solar cells.[16–21] Among all these studies, the most commonly used large organic spacer cations are butylammonium (BA) and phenethylammonium (PEA).[22] By mixing with other cations[23–27] or using additives such as NH_4SCN,[19,28,29] NH_4Cl,[19] or MACl,[30] the PV efficiency has been further improved to around 15% in BA- or PEA-based 2D perovskite solar cells.[19,24,25] Without mixing cations or using additives, BA-based 2D perovskite solar cells can still achieve relatively better efficiency, ≈12% for $<n>=4$ and 11% for $<n>=3$;[15] in contrast, PEA-based systems only achieved ≈7% for $<n>=3$ and ≈9% for $<n>=4$.[31] However, PEA-based 2D perovskites are more interesting from the perspective of introducing large functional conjugated organic cations into 2D perovskites,[32] because PEA is perhaps the smallest conjugated cation.

Performance of 2D perovskite solar cells can be affected by many factors, including surface morphology, phase composition,

Dr. L. Yan, Dr. J. Hu, N. Zhou, Prof. A. M. Moran, Prof. W. You
Department of Chemistry
University of North Carolina at Chapel Hill
Chapel Hill, NC 27599, USA
E-mail: wyou@unc.edu

The ORCID identification number(s) for the author(s) of this article can be found under https://doi.org/10.1002/solr.201900374.

DOI: 10.1002/solr.201900374

phase distribution, and crystal orientation of the perovskite films.[31] For PEA-based 2D perovskite solar cells, there are two outstanding issues that limit the device efficiency. First, PEA-based 2D perovskite films always have a significant amount of the $n = 1$ phase that has the largest band gap among all phases typically co-existing in 2D perovskite films and the slowest charge transport.[33] The limited absorption due to a large band gap, together with the slow charge transport, contributes significantly to the observed low power conversion efficiency for PEA-based 2D perovskite solar cells. Therefore, reducing or even eliminating the amount of $n = 1$ phase would be beneficial for further improvement of 2D perovskite-based solar cells. Second, the larger size of PEA could lead to more defects in the crystals, and therefore, more traps in the perovskite films; these traps act as charge recombination centers, causing a poor fill factor (*FF*). Thus, reducing the amount of traps is also important for the photovoltaic device performance.

It has been shown that adjusting the intermolecular interaction between organic cations in 2D perovskites can have significant impact on phase distribution, crystal orientation, and surface morphology.[34,35] Explored intermolecular interactions include the van der Waals interaction, aryl-perfluoroaryl interaction, and hydrogen bonding.[24,34,36–38] Promising results have been obtained. For example, we have recently discovered that the 2D perovskite-based solar cells with added perfluorophenethylammonium (F5-PEA) could significantly improve their stability while maintaining decent efficiency,[34] where the non-covalent interaction between PEA and F5-PEA has been identified as the key reason.

CH···π interaction is another strong, yet less explored (inter) molecular interaction,[39] which has never been investigated in 2D perovskites. During our ongoing investigation on tuning intermolecular interactions in 2D perovskites, we found that the CH···π interaction could be utilized to tune the compositions of different phases in PEA-based 2D perovskites. Specifically, replacing 50% of PEA cations with propylammonium cations (C3A) in the PEA-based 2D perovskites ($<n> = 3$) can selectively remove $n = 1$ phase. Furthermore, the C3A cations could passivate the defects (trap states) in PEA-based 2D perovskite films, likely due to the small size of C3A. Both effects – controlling phase composition and passivating the defects – enhanced the device efficiency of PEA-based 2D perovskite ($<n> = 3$) solar cells to the level of 10% with a 1:1 ratio of PEA:C3A. In contrast, the original PEA-based 2D perovskites solar cell only afforded an efficiency of ≈7.5%. Furthermore, these beneficial effects from C3A appear to be generally applicable to other aryl-derived cation-based 2D perovskites; specifically, we have observed efficiency enhancement for 2D perovskite solar cells based on thiophenethylammonium (TEA), 2-fluorophenethylammonium (oFPEA), or 3-fluorophenethylammonium (mFPEA).

2. Results and Discussion

2.1. Spectroscopic Evidence for Phase Control via Substituting PEA with C3A

Our original intention was to utilize a cation of small size to fill/passivate the trap states in PEA-based 2D perovskites, aiming to improve device performance.[26,27] In this regard, ethyl ammonium (C2A) would be a good choice; however, its small size would enable its incorporation into 3D perovskite structures without forming 2D phases.[40,41] Thus, we chose propyl ammonium (C3A), the smallest alkyl cation that can form 2D perovskites structure.[42] However, C3A might still introduce complications, because this cation can form not only normal Ruddlesden-Popper (RP) 2D perovskites[42] but also other type of perovskites.[40,43,44] Yet, the XRD patterns for our C3A-incorporated perovskites (*vide infra*) are different from those of other types of perovskites published earlier[40,43,44]; together with other evidence (*vide infra*), we believe that the perovskites studied here still belong to RP 2D perovskites. Nevertheless, as we will show below, the incorporation of C3A into PEA-based 2D perovskites not only passivates the defects, but it can also selectively remove the undesirable $n = 1$ phase.

As shown in **Figure 1**a, the PEA-based 2D perovskite ($<n> = 3$) film exhibits a rather strong $n = 1$ absorption peak, contrasting the negligible $n = 1$ absorption in BA-based ($<n> = 3$) film. Because the $n = 1$ phase has the largest band gap and lowest conductivity among all different n phases in 2D perovskites, ideally one should eliminate the $n = 1$ phase if these perovskites are intended for photovoltaic applications. Interestingly, after substituting C3A into PEA-based 2D perovskites ($<n> = 3$), i.e., replacing PEA with equal moles of C3A to maintain the average film composition ($<n> = 3$), the absorption intensity of the $n = 1$ phase gradually reduces (Figure 1a) as the amount of C3A increases, and completely vanishes at 50% substitution of C3A (C3A:PEA = 1:1). Further increasing the amount of C3A (i.e., 75%) results in the absorption profile closer to that of the pure C3A-based 2D perovskites (Figure 1a), where the absorption of different n phases becomes rather weak.

Because photoluminescence (PL) can be used to identify the phase composition and distribution,[20,31] we further measured the PL of our 2D perovskites ($<n> = 3$) on glass substrate from both the back and front sides to further confirm the impact of introducing C3A. At 0% C3A, one can clearly observe a strong PL signal for the $n = 1$ phase from both sides of the film (Figure 1b,c). As C3A amount increases, the PL from the $n = 1$ phase weakens and eventually disappears; this occurs at 25% C3A for the PL measured from the front side and 50% C3A for the PL measured from the back side. Thus, these PL data support the discovery from the UV-Vis measurement, i.e., substituting PEA with C3A can selectively remove the $n = 1$ phase in PEA-based 2D perovskites. Further evidence on the selective removal of the $n = 1$ phase by adding C3A comes from transient absorption (TA) measurement, a technique that has been used to identify the composition in 2D perovskite thin films.[45] As shown in Figure 1d, the TA signal for the $n = 1$ phase can be clearly identified for pure PEA-based 2D perovskites (with just 1 ps after pump excitation); in contrast, this signal disappears for the film with 50% C3A (i.e., C3A:PEA = 1:1).

2.2. Confirming Interaction with Model Compounds ($n = 1$) of Different C3A:PEA Ratios

To understand why substituting PEA with C3A leads to the selective removal of the $n = 1$ phase in PEA-based $<n> = 3$ perovskite films, we next investigated perovskites films of $n = 1$, which would allow to focus on the interactions between C3A and

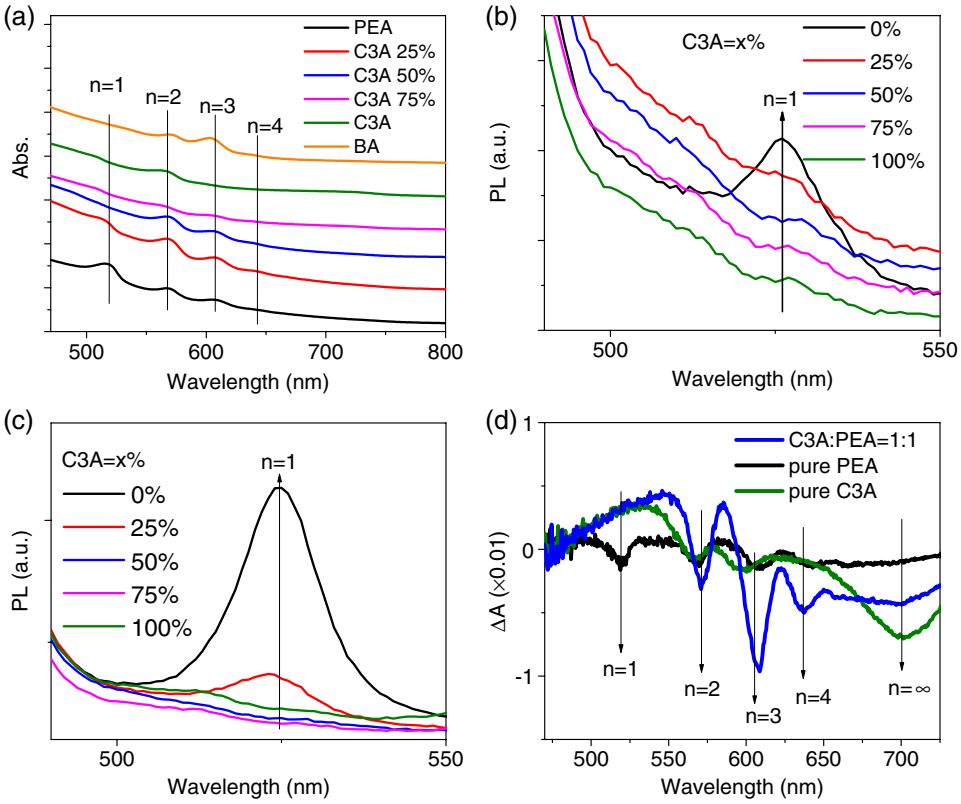

Figure 1. a) Absorption profiles of PEA, C3A, BA, and C3A:PEA mixed cation-based perovskites with <n> = 3, b) PL of front side (air) and c) back side (glass) of 2D perovskites with different C3A:PEA ratios, d) TA of a 2D perovskite film of pure PEA, pure C3A and C3A:PEA=1:1 with <n> = 3 at delay time of 1 ps.

PEA in the organic cation layer between lead iodide octahedra layers. **Figure 2**a shows that the absorption of the 50% C3A substitution (i.e., C3A:PEA = 1:1) has a distinctively different exciton peak than those of 0% and 100% C3A (i.e., pure PEA- and pure C3A-based perovskite films of $n = 1$, respectively), indicating the presence of a new 2D perovskite phase for 50% C3A, which is likely due to the interaction between C3A and PEA in the organic interlayer. This new phase from the C3A:PEA (1:1)-based 2D perovskite film ($n = 1$) can still be observed from the 25% C3A-based film, which has two absorption peaks, appearing to be a superposition of the absorption from 50% C3A and 0% C3A (i.e., pure PEA). On the other hand, the absorption spectrum of 75% C3A-based film is very similar to that of 100% C3A (i.e., pure C3A). These observations imply that further increasing the content of C3A beyond 50% could lead to disruption of the formation of C3A:PEA (1:1) perovskite phase.

Characterization of all these $n = 1$ films with powder X-ray diffraction (XRD) offers further evidence on the formation of the C3A:PEA (1:1) perovskite phase. For example, the XRD patterns in the small angle range (Figure 2b) clearly indicate that the 25% C3A-based film contains the original PEA phase (i.e., 0% C3A) and a new phase corresponding to the C3A:PEA (1:1) perovskite. On the other hand, the small angle peak for the 75% C3A-based film contains contributions from 0%, 50%, and 100% C3A-based perovskite phases, resulting in the broadening of this peak and shifting in position. It appears that the 75% C3A-based perovskite film ($n = 1$) has a significant amount of structural disorder, as further indicated by the rather broadened peaks in its XRD pattern in the large angle range (Figure S3, Supporting Information).

Taking all these results together, we propose that there is a strong interaction between C3A and PEA, likely through the CH···π interaction, which would account for the observed new perovskite phase in the C3A:PEA (1:1)-based film ($n = 1$) and the selective removal of the $n = 1$ phase in the PEA-based 2D perovskite film (<n> = 3) with 50% C3A substitution. Indeed, it has been well studied that there is a strong CH···π interaction between the methyl group and the benzene ring.[46–48] In our study, there is no CH···π interaction in pure C3A-based 2D perovskite films, because there are no π delocalized structures in the organic interlayers. In contrast, there is (sp^2) CH···π interaction in pure PEA-based 2D perovskite films, evidenced by analyzing the crystal structure of PEA_2PbI_4 ($n = 1$).[49] Specifically, in its crystal structure (Figure S5, Supporting Information), the smallest C–C distances between the benzene rings are 3.896 and 3.846 Å, and the corresponding H–C distances between adjunct benzene rings are about 3.047 and 3.008 Å, which are in the range of the intermolecular CH···π interaction (3.05 Å).[50] Further calculation of the angle and distance between the CH and π plane indicates the CH···π interaction exists in PEA_2PbI_4 according to the CH···π model by Nishio,[51] as shown in Table S1, Supporting Information.

Further evidence for the proposed CH···π interaction in our 2D perovskites comes from Fourier-transform infrared (FTIR)

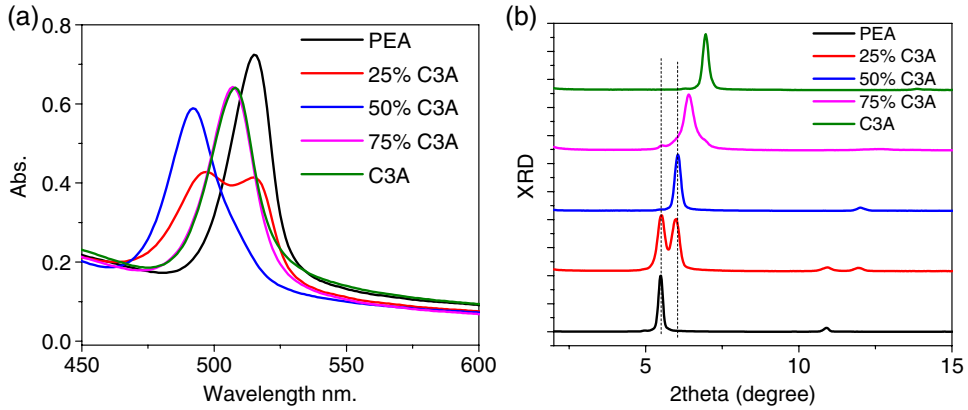

Figure 2. a) Absorption profiles and b) small angle range of XRD patterns of C3A:PEA-based 2D perovskites with $n = 1$.

study of these perovskite films ($n = 1$). It is known that for intermolecular CH···π interaction, there is a small shift to lower frequency for the C-H stretching band in the FTIR spectrum.[50] As shown in **Figure 3**, the sp^3 C–H stretching band for the methyl group in C3A-based perovskite films shifts from 2970 cm^{-1} (for pure C3A, $n = 1$) to 2963 cm^{-1} (for C3A:PEA = 1:1, $n = 1$),[52] indicating the intermolecular sp^3 CH···π interaction between the methyl group in C3A and the benzene π ring in PEA. On the other hand, sp^2 C–H stretching for the benzene ring in PEA-based perovskite films is located at 3019 cm^{-1} (for pure PEA, $n = 1$), which almost disappears for 50% C3A-based films (C3A:PEA = 1:1, $n = 1$). This indicates that the intermolecular CH···π interaction between the methyl group in C3A and the benzene π ring in PEA has largely replaced the previously existing PEA-PEA (CH···π) interaction in pure PEA-based perovskites ($n = 1$), given the 1:1 ratio of C3A to PEA.[39,47,53]

All these observations strongly support the proposed CH···π interaction between the methyl group in C3A and the benzene π ring in PEA in these mixed cation-based 2D perovskite films ($n = 1$). For the 2D perovskite films (<n> = 3), the clear observation of the $n = 1$ phase for pure PEA-based one is likely caused by the strong (sp^2) CH···π interaction between PEA molecules;

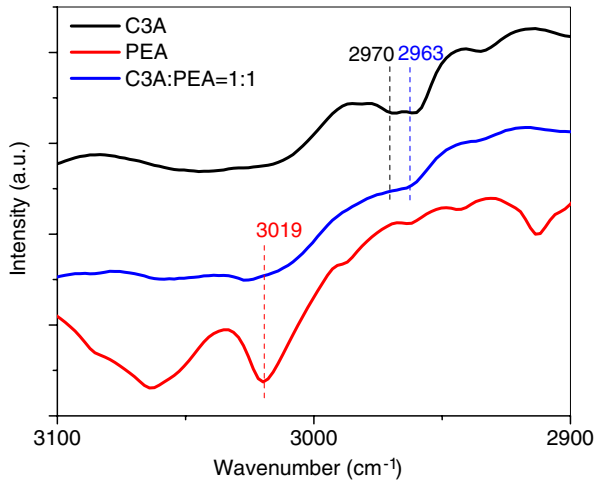

Figure 3. FTIR spectrum of a perovskite film with $n = 1$ based on pure C3A, pure PEA, and C3A:PEA=1:1 mixture.

similarly, no $n = 1$ phase was observed for pure C3A-based perovskite films, which can be ascribed to the absence of CH···π interaction. Regarding the absence of the $n = 1$ phase in the 1:1 mixed C3A and PEA-based 2D perovskites, we argue that the sp^3 CH···π interaction between the C3A and PEA is not strong enough to form the $n = 1$ phase. These results indicate that the CH···π interaction can play an important role in the phase formation in 2D perovskites; adjusting the CH···π interaction can be utilized to fine tune the phase composition in these 2D perovskite films.

2.3. Photovoltaic Device Performance of 2D Perovskites with Different C3A:PEA Ratios

Tuning the phase composition has a strong impact on the device performance of such 2D perovskite (<n> = 3)-based solar cells. As summarized in **Figure 4** and **Table 1**, the selective removal of the $n = 1$ phase in the case of 1:1 mixed cations of C3A and PEA-based 2D perovskites leads to appreciable improvement on the short circuit current density (J_{sc}) and fill factor (FF) of its solar cells, reaching an overall efficiency of ≈10%, which is a 30% improvement compared with the efficiency by the pure PEA-based solar cells. Given that the $n = 1$ phase has limited absorption due to a large band gap and slow charge transport, eliminating the $n = 1$ phase in the case of 50% C3A would lead to the observed enhancement of efficiency.

As we proposed previously, the substitution of C3A into PEA-based 2D perovskites could also remove defects (trap states) in the PEA-based perovskite due to the small size of C3A. To verify this hypothesis, we further measured the density of trap states in our 2D perovskites (<n> = 3) by using the space-charge-limited current (SCLC) technique[54,55] with a device structure of ITO/SnO_2/2D perovskite / PCBM/Bphen/Al. Specifically, the density of trap states was calculated according to Equation (1).

$$n_{trap} = \frac{2V_{TFL}\varepsilon\varepsilon_0}{eL^2} \quad (1)$$

where e is the element charge, L is the thickness of the film (350 nm), V_{TFL} is the trap-filled limit voltage (defined as the applied voltage at the kink point, where the current increases and becomes nonlinear), and ε_0 and ε are the permittivity of

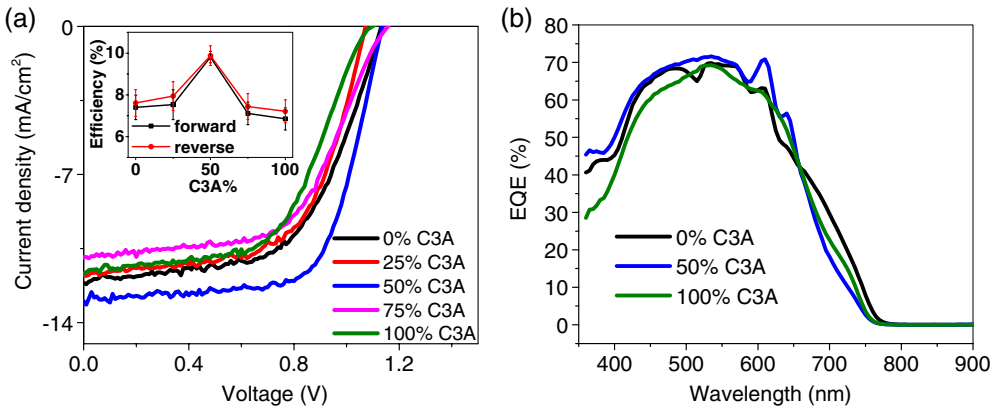

Figure 4. a) *J-V* curves of photovoltaic devices based on studied 2D perovskites; the inset is the C3A concentration-dependent efficiency, and b) EQE curves of perovskite solar cells with <n>=3.

Table 1. Photovoltaic device performance of C3A:PEA mixed cation-based 2D perovskites.

C3A%	Scan direction	J_{sc} [mA cm^{-2}]	V_{oc} [V]	*FF* [%]	η [%]
0%	Forward	12.00 ± 0.48	1.119 ± 0.017	55.2 ± 3.7	7.40 ± 0.59
	Reverse	11.92 ± 0.46	1.133 ± 0.011	56.4 ± 4.3	7.61 ± 0.64
25%	Forward	11.25 ± 0.74	1.071 ± 0.047	62.4 ± 1.2	7.53 ± 0.72
	Reverse	11.23 ± 0.79	1.057 ± 0.043	66.8 ± 1.6	7.94 ± 0.69
50%	Forward	12.91 ± 0.37	1.131 ± 0.011	67.2 ± 1.1	9.81 ± 0.28
	Reverse	12.86 ± 0.31	1.122 ± 0.014	68.5 ± 2.8	9.88 ± 0.47
75%	Forward	11.12 ± 0.97	1.154 ± 0.005	55.5 ± 1.3	7.11 ± 0.54
	Reverse	10.97 ± 0.94	1.153 ± 0.004	58.9 ± 3.2	7.44 ± 0.62
100%	Forward	11.47 ± 0.79	1.101 ± 0.030	54.3 ± 2.7	6.85 ± 0.53
	Reverse	11.49 ± 0.76	1.145 ± 0.010	54.8 ± 2.5	7.21 ± 0.55

vacuum and the relative permittivity of 2D perovskite, respectively; here, we just use 28.8 for all 2D perovskites.[56]

The measured dark *J–V* curves are shown in **Figure 5**, with which the extracted values of the density of trap states for these 2D perovskites are summarized in **Table 2**. Indeed, the density of trap states density monotonically decreases as the amount of C3A increases from 0% to 50%, consistent with the increasing *FF*. However, further increasing the amount of C3A to 75% and finally to 100% does not lead to further decrease of the density of trap states; yet, the fill factor of corresponding solar cells continues to decrease. Because the fill factor of the perovskite solar cells is also affected by other factors, such as the crystal grain size, it is likely that factors other than defect passivation also play important roles in these 2D perovskite solar cells, in particular, for the 75% C3A-based 2D perovskites (and also 100% C3A-based 2D perovskites).

2.4. Morphology of 2D Perovskite Films with Different C3A:PEA Ratios

To probe the crystallinity and crystal grain sizes, we further investigated our 2D perovskite films (<n> = 3) with XRD and AFM.

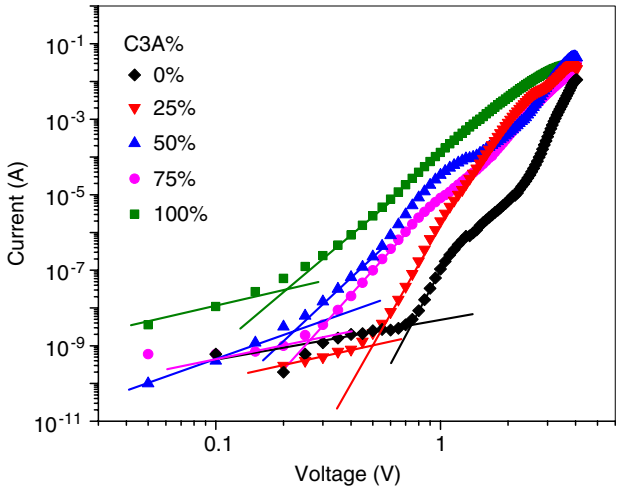

Figure 5. The trap state measurement for 2D perovskites with different C3A:PEA ratios.

Table 2. Trap state density in 2D perovskites with different C3A:PEA ratios.

C3A%	100%	75%	50%	25%	0%
V_{TFL} (V)	0.21	0.26	0.22	0.50	0.74
n_{trap} ($\times 10^{15}$cm^{-3})	5.45	6.75	5.71	12.99	19.22

For all these 2D perovskite films with different C3A:PEA ratios, we only observed strong (111) (202) peaks in their XRD patterns, as shown in **Figure 6**a, indicating highly orientated films, consistent with previous reports.[15] The 50% C3A-based 2D perovskite film has the smallest full width at half maximum (FWHM), as shown in Figure 6b, indicating largest crystalline grain size. Further increasing the amount of C3A to 75% and 100% leads to a larger FWHM, indicating smaller crystalline grain size. Small crystalline grains would impede the charge transport, thereby accounting for a lower fill factor in these 2D perovskite based solar cells.

The surface morphology of perovskites has a strong impact on device performance. We first applied scanning electron

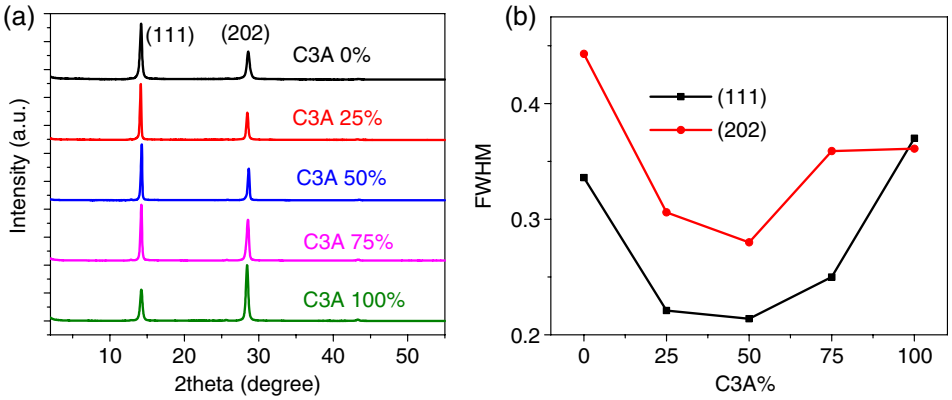

Figure 6. a) XRD patterns of 2D perovskite films of different C3A:PEA ratios, b) FWHM of (111) and (202) peak from 2D perovskite films of different C3A:PEA ratios.

microscope (SEM) to probe the surface. Unfortunately, the obtained SEM images (Figure S6, Supporting Information) do not show sufficient contrast between the grain boundaries and the grains, precluding us from observing the grain size. Similar observations have been reported for 2D perovskite films in our previous study.[31] Nevertheless, we observed difference in the size and density of pinholes among these 2D perovskites films. In short, the surface morphology of the 2D perovskite film becomes better as the amount of C3A increases. For example, we observed many large pinholes with 25% C3A-based perovskite film, while the 50% C3A-based film showed smaller pinholes. Interestingly, 75% C3A- and pure C3A-based perovskite films did not show much sign of pinholes (almost pinhole-free). Though obscured by the pinholes, we believe that the better surface morphology for 50% C3A-based film also contributes to the better *FF* for 50% C3A-based 2D perovskite solar cells than the ones with lower C3A amount (i.e., pure PEA and 25% C3A).

Further probing the surface morphology via AFM indicates that the films of 2D perovskites with low C3A amount (i.e., 0%, 25%, and 50% C3A) exhibit similar surface roughness (**Figure 7**). In contrast, the films with high amount of C3A (i.e., 75% and 100% C3A) are smoother. Furthermore, it can be observed from these AFM images that the grain sizes for the film having higher amount of C3A (75% and 100%) are visibly smaller than the ones having lower amount of C3A (0%, 25%, and 50%), which is consistent with the trend determined by FWHM with XRD measurements.

These results point to another important factor that affects the photovoltaic device efficiency of 2D perovskites: the size of the crystalline grains. In earlier section, we demonstrate that further

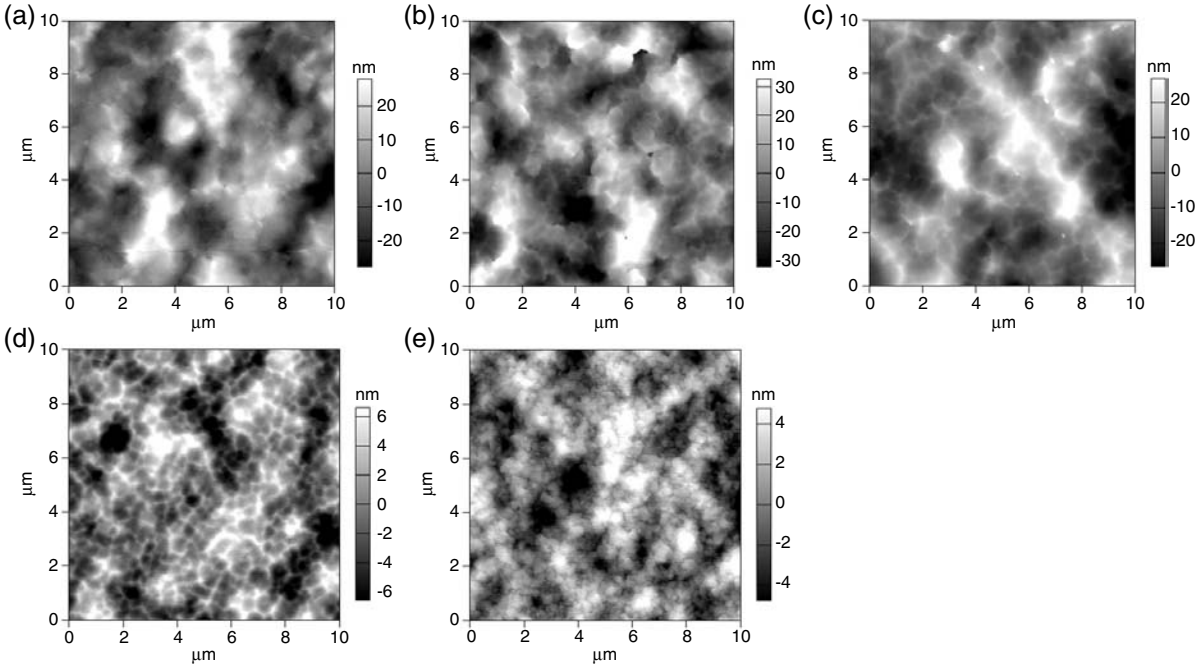

Figure 7. AFM height images of 2D perovskites of different C3A:PEA ratios: a) 0% C3A (pure PEA), b) 25% C3A, c) 50% C3A, d) 75% C3A and e) 100% C3A (pure C3A). The average roughness values are a) 13.491 nm, b) 15.964 nm, c) 12.817 nm, d) 3.264 nm, and e) 2.352 nm.

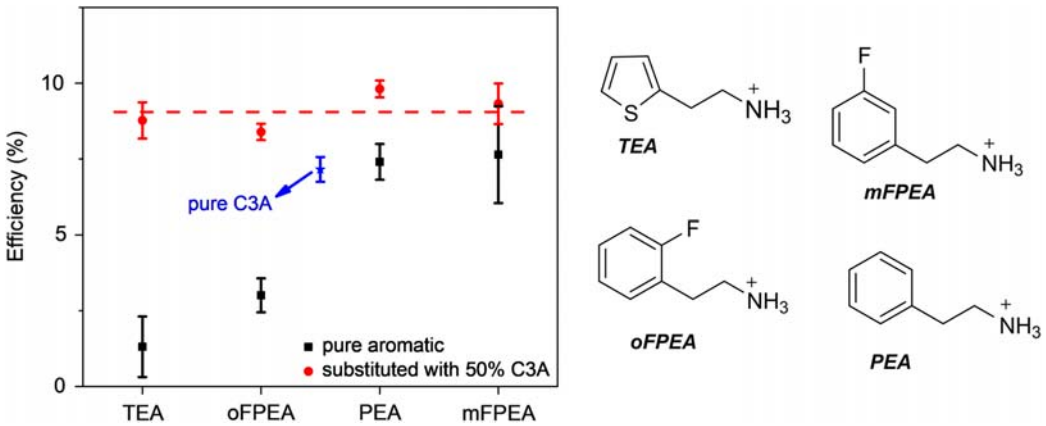

Figure 8. Photovoltaic device efficiency enhancement of 2D perovskites with $<n> = 3$ for PEA, oF1PEA, mF1PEA, and TEA after substituting 50% C3A. The chemical structures of these aromatic ammoniums are also listed.

increase of C3A from 50% to 75% and 100% offers similar passivation effect, i.e., low density of trap states, which would lead to similar *FF* values of the PV devices for 50%, 75%, and 100% C3A-based 2D perovskites; however, as we show in this section, as the amount of C3A increases from 50% to 100%, the crystal grain size in 2D perovskite films becomes smaller, which would impede charge transport and result in low *FF*. For these reasons, the 2D perovskite film with 50% C3A incorporation shows the best FF in our study, because it has both low density trap states and large crystal grain size.

2.5. 2D RP Perovskite Solar Cells by Mixing C3A with Other Aromatic Cations

Because the CH···π interaction should exist between C3A and other aromatic ammonium cations, we next tested whether substituting C3A into other aromatic ammonium cation-based 2D perovskites would offer similar performance enhancement in their solar cells. To our delight, a noticeable enhancement of efficiency (and even significant in some cases) was observed for all studied aromatic cation-based 2D perovskite ($<n> = 3$) solar cells after substituting 50% C3A into the film (**Figure 8**), when compared with the pure aromatic cation-based ones *and* the pure C3A-based ones. These encouraging results indicate that this new approach of tuning CH···π interaction could be a rather universal approach to enhance efficiency of aromatic cation-based 2D perovskite solar cells.

3. Conclusion

The CH···π interaction is a weak non-covalent interaction and often overpowered by other stronger interactions in given organic molecules; yet, it can play an important role in fine-tuning intermolecular interactions in the solid state, which, as we show here, has a significant impact on the phase composition of 2D perovskites. Substituting 50% C3A into PEA-based 2D perovskites can a) selectively remove the $n = 1$ phase, which helps to improve film absorption and charge transport b) passivate the trap states, and c) improve the morphology with larger crystalline grain size. All these contribute to the much improved photovoltaic device efficiency (≈10%) for the 1:1 C3A:PEA-based 2D perovskites ($<n> = 3$), a 30% increase over pure PEA-based ones. Because the tuning of CH···π interaction is not specific to the studied C3A and PEA, other aromatic ammonium cations can also have similar CH···π interaction with C3A and enjoy similar benefits, leading to observed photovoltaic performance increase in these cation-based 2D perovskites. The fact that all devices reaching similar level of efficiency (≈10%), independent of the chemical nature of aromatic units and the starting device efficiency based on pure aromatic cation-based 2D perovskites, implies that a) this method could be rather universal and b) the CH···π interaction must be the deciding underlying factor in achieving high device performance.

Supporting Information

Supporting Information is available from the Wiley Online Library or from the author.

Acknowledgements

L.Y., J.H., and W.Y. were supported by the National Science Foundation (DMR-1728921) and UNC Research Opportunities Initiative (ROI) through the Center of Hybrid Materials Enabled Electronic Technology and the Center for Hybrid Organic Inorganic Semiconductors for Energy (CHOISE), an Energy Frontier Research Center funded by the U.S. Department of Energy (DOE), Office of Science, Office of Basic Energy Sciences (BES). FTIR, XRD, SEM, and AFM in this work was performed in part at the Chapel Hill Analytical and Nanofabrication Laboratory, CHANL, a member of the North Carolina Research Triangle Nanotechnology Network, RTNN, which is supported by the National Science Foundation, Grant ECCS-1542015, as part of the National Nanotechnology Coordinated Infrastructure, NNCI. L.Y. and W.Y. thank Stephanie Samson, Sara Wehlin, and Professor Gerald Meyer (UNC-Chapel Hill) for assistance with PL measurements. N.Z. and A.M.M. were supported by the National Science Foundation (CHE-1763207).

Conflict of Interest

The authors declare no conflict of interest.

Keywords

2D organic inorganic hybrid perovskites, CH···π interaction, solar cells

Received: August 27, 2019
Revised: October 3, 2019
Published online: October 31, 2019

[1] J. Hu, L. Yan, W. You, *Adv. Mater.* **2018**, *30*, 1802041.
[2] G. Grancini, M. K. Nazeeruddin, *Nat. Rev. Mater.* **2019**, *4*, 4.
[3] Y. Zheng, T. Niu, X. Ran, J. Qiu, B. Li, Y. Xia, Y. Chen, W. Huang, *J. Mater. Chem. A* **2019**, *7*, 13860.
[4] L. N. Quan, M. Yuan, R. Comin, O. Voznyy, E. M. Beauregard, S. Hoogland, A. Buin, A. R. Kirmani, K. Zhao, A. Amassian, D. H. Kim, E. H. Sargent, *J. Am. Chem. Soc.* **2016**, *138*, 2649.
[5] Y. Lin, Y. Bai, Y. Fang, Z. Chen, S. Yang, X. Zheng, S. Tang, Y. Liu, J. Zhao, J. Huang, *J. Phys. Chem. Lett.* **2018**, *9*, 654.
[6] Q. Jiang, Y. Zhao, X. Zhang, X. Yang, Y. Chen, Z. Chu, Q. Ye, X. Li, Z. Yin, J. You, *Nat. Photonics* **2019**, *13*, 460.
[7] W. Xu, Q. Hu, S. Bai, C. Bao, Y. Miao, Z. Yuan, T. Borzda, A. J. Barker, E. Tyukalova, Z. Hu, M. Kawecki, H. Wang, Z. Yan, X. Liu, X. Shi, K. Uvdal, M. Fahlman, W. Zhang, M. Duchamp, J.-M. Liu, A. Petrozza, J. Wang, L.-M. Liu, W. Huang, F. Gao, *Nat. Photonics* **2019**, *13*, 418.
[8] K. Lin, J. Xing, L. N. Quan, F. P. G. de Arquer, X. Gong, J. Lu, L. Xie, W. Zhao, D. Zhang, C. Yan, W. Li, X. Liu, Y. Lu, J. Kirman, E. H. Sargent, Q. Xiong, Z. Wei, *Nature* **2018**, *562*, 245.
[9] C. R. Kagan, D. B. Mitzi, C. D. Dimitrakopoulos, A. R. Brown, A. Pomp, C. M. Hart, D. M. D. Leeuw, S. F. Nelson, Y. Y. Lin, D. J. Gundlach, T. N. Jackson, P. T. Herwig, K. Müllen, G. Horowitz, D. Fichou, X. Peng, Z. Xu, F. Garnier, B. Furman, T. Graham, S. Hegde, S. Purushothaman, J. H. Burroughes, C. A. Jones, R. H. Friend, A. Tsumura, H. Koezuka, T. Ando, Z. Bao, A. Dodabalapur, A. J. Lovinger, C. P. Jarrett, M. Matters, R. Hajlaoui, A. Yassar, P. Srivastava, J. Kymissis, A. Callegari, J. M. Shaw, C. A. Feild, Z. Schlesinger, R. B. Laibowitz, W. T. A. Harrison, A. M. Guloy, C. Q. Xu, K. Liang, M. T. Prikas, M. Era, T. Hattori, T. Taira, T. Tsutsui, K. Chondroudis, G. C. Papavassiliou, I. B. Koutselas, A. Terzis, M. H. Whangbo, M. Shur, M. Hack, J. G. Shaw, L. Torsi, H. E. Katz, *Science* **1999**, *286*, 945.
[10] D. B. Mitzi, C. A. Feild, W. T. A. Harrison, A. M. Guloy, *Nature* **1994**, *369*, 467.
[11] T. Matsushima, F. Mathevet, B. Heinrich, S. Terakawa, T. Fujihara, C. Qin, A. S. D. Sandanayaka, J.-C. Ribierre, C. Adachi, *Appl. Phys. Lett.* **2016**, *109*, 253301.
[12] T. Matsushima, S. Hwang, A. S. D. Sandanayaka, C. Qin, S. Terakawa, T. Fujihara, M. Yahiro, C. Adachi, *Adv. Mater.* **2016**, *28*, 10275.
[13] Y. Chen, Y. Sun, J. Peng, J. Tang, K. Zheng, Z. Liang, *Adv. Mater.* **2018**, *30*, 1703487.
[14] D. H. Cao, C. C. Stoumpos, O. K. Farha, J. T. Hupp, M. G. Kanatzidis, *J. Am. Chem. Soc.* **2015**, *137*, 7843.
[15] H. Tsai, W. Nie, J.-C. Blancon, C. C. Stoumpos, R. Asadpour, B. Harutyunyan, A. J. Neukirch, R. Verduzco, J. J. Crochet, S. Tretiak, L. Pedesseau, J. Even, M. A. Alam, G. Gupta, J. Lou, P. M. Ajayan, M. J. Bedzyk, M. G. Kanatzidis, A. D. Mohite, *Nature* **2016**, *536*, 312.
[16] A. H. Proppe, R. Quintero-Bermudez, H. Tan, O. Voznyy, S. O. Kelley, E. H. Sargent, *J. Am. Chem. Soc.* **2018**, *140*, 2890.
[17] N. Zhou, Y. Shen, L. Li, S. Tan, N. Liu, G. Zheng, Q. Chen, H. Zhou, *J. Am. Chem. Soc.* **2018**, *140*, 459.
[18] C. Ma, D. Shen, T.-W. Ng, M.-F. Lo, C.-S. Lee, *Adv. Mater.* **2018**, *30*, 1800710.
[19] W. Fu, J. Wang, L. Zuo, K. Gao, F. Liu, D. S. Ginger, A. K. Y. Jen, *ACS Energy Lett.* **2018**, *3*, 2086.
[20] J. Liu, J. Leng, K. Wu, J. Zhang, S. Jin, *J. Am. Chem. Soc.* **2017**, *139*, 1432.
[21] J. Qiu, Y. Zheng, Y. Xia, L. Chao, Y. Chen, W. Huang, *Adv. Funct. Mater.* **2018**, 1806831, https://doi.org/10.1002/adfm.201806831.
[22] I. C. Smith, E. T. Hoke, D. Solis-Ibarra, M. D. McGehee, H. I. Karunadasa, *Angew. Chem., Int. Ed.* **2014**, *53*, 11232.
[23] X. Zhang, X. Ren, B. Liu, R. Munir, X. Zhu, D. Yang, J. Li, Y. Liu, D.-M. Smilgies, R. Li, Z. Yang, T. Niu, X. Wang, A. Amassian, K. Zhao, S. Liu, *Energy Environ. Sci.* **2017**, *10*, 2095.
[24] M. Long, T. Zhang, D. Chen, M. Qin, Z. Chen, L. Gong, X. Lu, F. Xie, W. Xie, J. Chen, J. Xu, *ACS Energy Lett.* **2019**, *4*, 1025.
[25] X. Lian, J. Chen, M. Qin, Y. Zhang, T. Shuoxun, X. Lu, G. Wu, H. Chen, *Angew. Chem.* **2019**, *131*, 9509.
[26] S. Tan, N. Zhou, Y. Chen, L. Li, G. Liu, P. Liu, C. Zhu, J. Lu, W. Sun, Q. Chen, H. Zhou, *Adv. Energy Mater.* **2019**, *9*, 1803024.
[27] J. Qiu, Y. Xia, Y. Zheng, W. Hui, H. Gu, W. Yuan, H. Yu, L. Chao, T. Niu, Y. Yang, X. Gao, Y. Chen, W. Huang, *ACS Energy Lett.* **2019**, *4*, 1513.
[28] X. Zhang, G. Wu, W. Fu, M. Qin, W. Yang, J. Yan, Z. Zhang, X. Lu, H. Chen, *Adv. Energy Mater.* **2018**, *8*, 1702498.
[29] X. Zhang, G. Wu, S. Yang, W. Fu, Z. Zhang, C. Chen, W. Liu, J. Yan, W. Yang, H. Chen, *Small* **2017**, *13*, 1700611.
[30] J. Qing, X.-K. Liu, M. Li, F. Liu, Z. Yuan, E. Tiukalova, Z. Yan, M. Duchamp, S. Chen, Y. Wang, S. Bai, J.-M. Liu, H. J. Snaith, C.-S. Lee, T. C. Sum, F. Gao, *Adv. Energy Mater.* **2018**, *8*, 1800185.
[31] L. Yan, J. Hu, Z. Guo, H. Chen, M. F. Toney, A. M. Moran, W. You, *ACS Appl. Mater. Interfaces* **2018**, *10*, 33187.
[32] C. Liu, W. Huhn, K.-Z. Du, A. Vazquez-Mayagoitia, D. Dirkes, W. You, Y. Kanai, D. B. Mitzi, V. Blum, *Phys. Rev. Lett.* **2018**, *121*, 146401.
[33] M. C. Gélvez-Rueda, E. M. Hutter, D. H. Cao, N. Renaud, C. C. Stoumpos, J. T. Hupp, T. J. Savenije, M. G. Kanatzidis, F. C. Grozema, *J. Phys. Chem. C* **2017**, *121*, 26566.
[34] J. Hu, I. W. H. Oswald, H. Hu, S. J. Stuard, M. M. Nahid, L. Yan, Z. Chen, H. Ade, J. R. Neilson, W. You, *ACS Mater. Lett.* **2019**, *1*, 171.
[35] J. Hu, I. W. H. Oswald, S. J. Stuard, M. M. Nahid, N. Zhou, O. F. Williams, Z. Guo, L. Yan, H. Hu, Z. Chen, X. Xiao, Y. Lin, Z. Yang, J. Huang, A. M. Moran, H. Ade, J. R. Neilson, W. You, *Nat. Commun.* **2019**, *10*, 1276.
[36] D. B. Mitzi, D. R. Medeiros, P. R. L. Malenfant, *Inorg. Chem.* **2002**, *41*, 2134.
[37] Z. Xu, D. B. Mitzi, *Chem. Mater.* **2003**, *15*, 3632.
[38] J. V. Milić, J.-H. Im, D. J. Kubicki, A. Ummadisingu, J.-Y. Seo, Y. Li, M. A. Ruiz-Preciado, M. I. Dar, S. M. Zakeeruddin, L. Emsley, M. Grätzel, *Adv. Energy Mater.* **2019**, *9*, 1900284.
[39] M. Nishio, *Phys. Chem. Chem. Phys.* **2011**, *13*, 13873.
[40] M. Safdari, A. Fischer, B. Xu, L. Kloo, J. M. Gardner, *J. Mater. Chem. A* **2015**, *3*, 9201.
[41] J.-H. Im, J. Chung, S.-J. Kim, N.-G. Park, *Nanoscale Res. Lett.* **2012**, *7*, 353.
[42] P. Cheng, Z. Xu, J. Li, Y. Liu, Y. Fan, L. Yu, D.-M. Smilgies, C. Müller, K. Zhao, S. F. Liu, *ACS Energy Lett.* **2018**, *3*, 1975.
[43] Y. Zhang, F. Li, K.-J. Jiang, J.-H. Huang, H. Wang, H. Fan, P. Wang, C.-M. Liu, L.-P. Zhang, Y. Song, *J. Mater. Chem. A* **2018**, *6*, 17867.
[44] J. M. Hoffman, X. Che, S. Sidhik, X. Li, I. Hadar, J.-C. Blancon, H. Yamaguchi, M. Kepenekian, C. Katan, J. Even, C. C. Stoumpos, A. D. Mohite, M. G. Kanatzidis, *J. Am. Chem. Soc.* **2019**, *141*, 10661.
[45] R. Quintero-Bermudez, A. Gold-Parker, A. H. Proppe, R. Munir, Z. Yang, S. O. Kelley, A. Amassian, M. F. Toney, E. H. Sargent, *Nat. Mater.* **2018**, *17*, 900.

[46] A. Fujii, H. Hayashi, J. W. Park, T. Kazama, N. Mikami, S. Tsuzuki, *Phys. Chem. Chem. Phys.* **2011**, *13*, 14131.
[47] S. Tsuzuki, K. Honda, T. Uchimaru, M. Mikami, K. Tanabe, *J. Am. Chem. Soc.* **2000**, *122*, 3746.
[48] M. J. Plevin, D. L. Bryce, J. Boisbouvier, *Nat. Chem.* **2010**, *2*, 466.
[49] K.-Z. Du, Q. Tu, X. Zhang, Q. Han, J. Liu, S. Zauscher, D. B. Mitzi, *Inorg. Chem.* **2017**, *56*, 9291.
[50] M. Nishio, M. Hirota, Y. Umezawa, *The CH/π Interaction: Evidence, Nature, and Consequences*, Wiley, New York / Chichester, UK **1998**.
[51] M. Nishio, Y. Umezawa, J. Fantini, M. S. Weiss, P. Chakrabarti, *Phys. Chem. Chem. Phys.* **2014**, *16*, 12648.
[52] T. Glaser, C. Müller, M. Sendner, C. Krekeler, O. E. Semonin, T. D. Hull, O. Yaffe, J. S. Owen, W. Kowalsky, A. Pucci, R. Lovrinčić, *J. Phys. Chem. Lett.* **2015**, *6*, 2913.
[53] S. K. Nayak, R. Sathishkumar, T. N. G. Row, *CrystEngComm* **2010**, *12*, 3112.
[54] D. Shi, V. Adinolfi, R. Comin, M. Yuan, E. Alarousu, A. Buin, Y. Chen, S. Hoogland, A. Rothenberger, K. Katsiev, Y. Losovyj, X. Zhang, P. A. Dowben, O. F. Mohammed, E. H. Sargent, O. M. Bakr, *Science* **2015**, *347*, 519.
[55] J. Jiang, Z. Jin, F. Gao, J. Sun, Q. Wang, S. Liu, *Adv. Sci.* **2018**, *5*, 1800474.
[56] A. Poglitsch, D. Weber, *J. Chem. Phys.* **1987**, *87*, 6373.